

Spatiotemporal seismicity pattern of the Taiwan orogen

Yi-Ying Wen^{1,2*}, Chien-Chih Chen^{3,4}, Strong Wen^{1,2}, and Wei-Tsen Lu¹

¹Department of Earth and Environmental Sciences, National Chung Cheng University, Chia-yi County 62102, Taiwan

²Environment and Disaster Monitoring Center, National Chung Cheng University, Chia-yi County 62102, Taiwan

³Department of Earth Sciences, National Central University, Taoyuan City 32001, Taiwan

⁴Earthquake-Disaster & Risk Evaluation and Management Center, National Central University, Taoyuan City 32001, Taiwan

Correspondence: Yi-Ying Wen (yiyingwen@ccu.edu.tw)

Abstract

We investigate the temporal and spatial seismicity patterns prior to eight $M > 6$ events nucleating in different regions of Taiwan through a region-time-length algorithm and an analysis of a self-organizing spinodal model. Our results show that the spatiotemporal seismicity variations during the preparation process of impending earthquakes display distinctive patterns corresponding to tectonic settings. Q-type events occur in southern Taiwan and experience a seismic quiescence stage prior to the mainshock. A seismicity decrease of $2.5 < M < 4.5$ events occurs around the relatively high b-value southern Central Range, which contributes to the accumulation of tectonic stress for preparing for the occurrence of the Q-type event. On the other hand, A-type events occur in central Taiwan and experience a seismic activation stage prior to the mainshock, which nucleates on the edge of the seismic activation area. We should pay attention when accelerating seismicity of $3 < M < 5$ events appears within the low b-value area, which could promote the nucleation process of the A-type event.

30 **1. Introduction**

31 Seismic activity is related to spatiotemporal variations in the stress field and state,
32 and seismicity changes prior to a large earthquake have been widely observed through
33 different techniques, e.g., b-value analysis (Chan et al., 2012; Wyss and Stefansson,
34 2006), noncritical precursory accelerating seismicity theory (PAST) (Mignan and
35 Giovambattista, 2008), pattern informatics (PI) algorithm (Rundle et al., 2003; Chen et
36 al., 2005), the region-time-length (RTL) algorithm (Chen and Wu, 2006; Wen et al.,
37 2016), and the analysis of self-organizing spinodal (SOS) model (Rundle et al., 2000).
38 Previous studies have mostly focused on a significant earthquake; therefore, it is not
39 easy to understand whether the properties of seismic activation and quiescence patterns
40 respond to regional tectonic stress.

41 The Taiwan orogenic belt, which is an active and ongoing arc–continent collision
42 zone as a result of the Philippine Sea Plate (PSP) obliquely colliding with the Eurasian
43 Plate (EP), is particularly complex due to the two adjacent subduction zones, the Ryukyu
44 trench and Manila trench to the northeast and south of the island, respectively (Suppe,
45 1984; Yu et al., 1997). The frequent and significant seismic activities as well as a rapid
46 convergence rate of 85 to 90 mm/yr are well observed by the island-wide GPS and
47 seismic networks (Fig. 1). The growth of the Taiwan orogenic belt shows propagation
48 from north to south due to oblique plate convergence and opposing subduction in the
49 southern and northern parts of Taiwan (Suppe, 1984). The central part of Taiwan, which
50 is experiencing rapid to full collision, mainly consists of the Coastal Range, Central
51 Range and Western Foothills (Shyu et al., 2005a; b). A myriad of active and thin-skinned
52 structures are the products of the accretion of the continental sliver to the continental
53 margin. In southern Taiwan, the EP subducting eastward beneath the PSP is in a stage
54 of incipient arc–continent collision (Kao et al., 2000; Shyu et al., 2005a; b). The

55 northwest domain of southern Taiwan, which represent the southern tip of the fold-and-
56 thrust belt in the coastal plain and foothill region and show very low seismicity, mainly
57 consist of Miocene shallow marine deposits and a Pliocene–Pleistocene foreland basin
58 as well as mudstones.

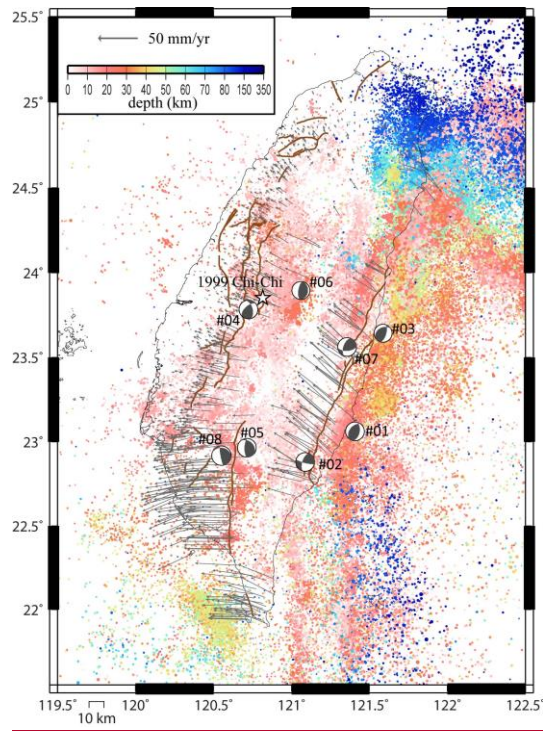


Figure 1: Horizontal velocities from 2002 to 2017 (Chen et al., 2018) and seismicity between 1991 and 2018. The white star shows the location of the 1999 Chi-Chi earthquake, and the ~~black stars~~ focal mechanisms determined by the [Global CMT solution](#) represent the locations of the investigated events in this study. The active faults (thick lines) identified by the Central Geological Survey of Taiwan are also shown.

59
60 Over the last two decades, several moderate earthquakes have occurred with various
61 seismicity patterns and in GPS velocity field regions. We investigate the temporal and
62 spatial seismicity patterns prior to eight $M > 6$ events nucleated in different regions of
63 Taiwan through the RTL algorithm and analysis of the SOS model. Our attempt is not

64 to catch the seismic precursor but to focus on the seismicity changes related to the
 65 regional tectonics, which might become useful hints for potential seismic hazard
 66 assessments. The results show that the temporal and spatial seismicity ($2.5 < M < 5$)
 67 variations during the preparation process of impending earthquakes could display
 68 distinctive patterns corresponding to the tectonic setting.

69

70 2. RTL Algorithm and Data

71 The region-time-length (RTL) algorithm (Sobolev and Tyupkin, 1997; 1999) is a
 72 statistical technique to detect the occurrence of seismic quiescence and activation by
 73 taking into account the location, occurrence time and magnitude of earthquakes. The
 74 RTL value is defined as the product of the three dimensionless factors, R , T and L :

$$75 \quad R(x, y, z, t) = \left[\sum_{i=1}^n \exp\left(-\frac{r_i}{r_0}\right) \right] - R_{bk}(x, y, z, t) \quad (1)$$

$$76 \quad T(x, y, z, t) = \left[\sum_{i=1}^n \exp\left(-\frac{t-t_i}{t_0}\right) \right] - T_{bk}(x, y, z, t) \quad (2)$$

$$77 \quad L(x, y, z, t) = \left[\sum_{i=1}^n \left(\frac{l_i}{r_i}\right) \right] - L_{bk}(x, y, z, t) \quad (3)$$

78 where r_i is the distance between the investigated point (x, y, z) and the i th prior event
 79 (with the occurrence time t_i and rupture length l_i). n is the number of prior events that
 80 occurred in a defined space–time window with $r_i \leq 2r_0$ (r_0 , characteristic distance) and
 81 $(t - t_i) \leq 2t_0$ (t_0 , characteristic time-span). Rupture length l_i is a function of
 82 earthquake magnitude (M_i), $\log l_i = 0.5M_i - 1.8$ (Kasahara, 1981). The weighted RTL
 83 value reflects the deviation from the background seismicity level (R_{bk} , T_{bk} and L_{bk}) with
 84 negative values for seismic quiescence and positive values for activation. r_0
 85 characterizes the decreasing influence of more distant events, and t_0 describes the
 86 reducing influence rate of the preceding events as the time of calculation moving on. To
 87 diminish the ambiguity in determining the characteristic parameters, we follow the

88 systematic procedure of correlation analysis over pairs of RTL results proposed by
89 Huang and Ding (2012) to obtain the optimal model parameters, \tilde{r}_0 and \tilde{t}_0 , of each
90 event. Details of this technique of correlation analysis are described in Appendix A. We
91 calculate various combinations of r_0 (ranging between 25 and 80 km with a step of 2.5
92 km) and t_0 (ranging between 0.25 and 2.0 yr with a step of 0.05 yr). As the correlation
93 coefficient criterion C_0 is set, we can calculate the ratio W (or weight) of the combination
94 with correlation coefficients equal to or larger than C_0 for each model parameter of r_{0i}
95 ($i=1\sim m; m=23$) and t_{0j} ($j=1\sim n; n=36$).

96 After testing many criterion sets, the criterion coefficient $C_0=0.6$ and criterion ratio
97 $W_0=0.5$ are acceptable for each event, which represents at least 50% of the total
98 combination pairs with correlation coefficient $C \geq C_0=0.6$. Then, we obtain the average
99 $\tilde{r}_0=49.6$ km and average $\tilde{t}_0=1.16$ yr. These model parameters are similar to those of
100 previous studies for Taiwan (Chen and Wu, 2006; Wen et al., 2016; Lu, 2017; Wen and
101 Chen, 2017).

102 For statistical analyses, catalog completeness is an important factor. Since 1991,
103 the Taiwan Telemetered Seismographic Network (TTSN) (Wang, 1989) has merged
104 with the Central Weather Bureau (CWB) seismic network and updated to an integrated
105 earthquake observation system, named the Central Weather Bureau Seismic Network
106 (CWBSN). Wang et al. (1994) pointed out that most shallow earthquakes occurring in
107 Taiwan are distributed at depths less than 35 km. According to previous studies (Wu
108 and Chiao, 2006; Wu et al., 2008; Wen et al., 2016; Hsu et al., 2021), we used the
109 earthquake catalog maintained by the CWB for the entire Taiwan area with $M \geq 2.5$ and
110 $\text{depth} \leq 35$ km between 1991 and 2018 and applied a declustering procedure proposed by
111 Gardner and Knopoff (1974). Considering a sufficient background seismicity and
112 minimizing the influence of the 1999 Chi-Chi earthquake, we only selected the $M > 6$

113 inland earthquakes between 2003 and 2016 in Taiwan. Since two events occurring in a
 114 close space–time window would show high similarity in RTL function (Lu, 2017), we
 115 excluded the event occurring within $2\tilde{r}_0$ and \tilde{r}_0 with respect to the last $M>6$ events. For
 116 example, two $M>6$ events within a distance of 10 km struck the Nantou area on 27
 117 March 2013 and 02 June 2013, and we only analyzed the former event. Therefore, we
 118 have eight qualified $M>6$ events, as listed in Table 1.

119

120 **Table 1:** Earthquake parameters for the investigated events determined by the CWB.

No.	Date (UT)	Long. (deg.)	Lat. (deg.)	Depth (km)	M_L
1	2003/12/10 04:38:14	121.398	23.067	17.7	6.4
2	2006/04/01 10:02:20	121.081	22.884	7.2	6.2
3	2009/10/03 17:36:06	121.579	23.648	29.2	6.1
4	2009/11/05 09:32:58	120.719	23.789	24.1	6.2
5	2010/03/04 00:18:52	120.707	22.969	22.6	6.4
6	2013/03/27 02:03:20	121.053	23.902	19.4	6.1
7	2013/10/31 12:02:10	121.349	23.566	15.0	6.4
8	2016/02/05 19:57:26	120.544	22.922	14.6	6.6

121

122 3. Results

123 3.1 Temporal seismicity variation

124 The temporal variation in the RTL function represents the different stages of
 125 seismicity rate change at the target location with respect to the background level. For
 126 consistency, we adopt a 10-year catalog as the background for each investigated event.
 127 Figure 2 shows the temporal variation in the RTL functions prior to the investigated
 128 events. We can see that before the occurrence of the investigated event, both seismicity
 129 changes are observed: the seismic quiescence stage for Nos. 1, 2, 5 and 8 (Q-type events

130 hereafter) and the seismic activation stage for Nos. 3, 4, 6 and 7 (A-type events hereafter).
 131 Q-type events occurred at different locations in southern Taiwan, and most, 3 among 4,
 132 of their temporal RTL functions exhibit the seismic quiescence stages during 2002–
 133 2004, which was before the occurrence of the 2003 Chengkung earthquake, i.e., event
 134 No. 1. The seismicity increase (activation stage) took approximately two years following
 135 the 2003 Chengkung mainshock (event No. 1). We note that the length of the seismic
 136 quiescence stage prior to the Q-type event might correspond to the magnitude.

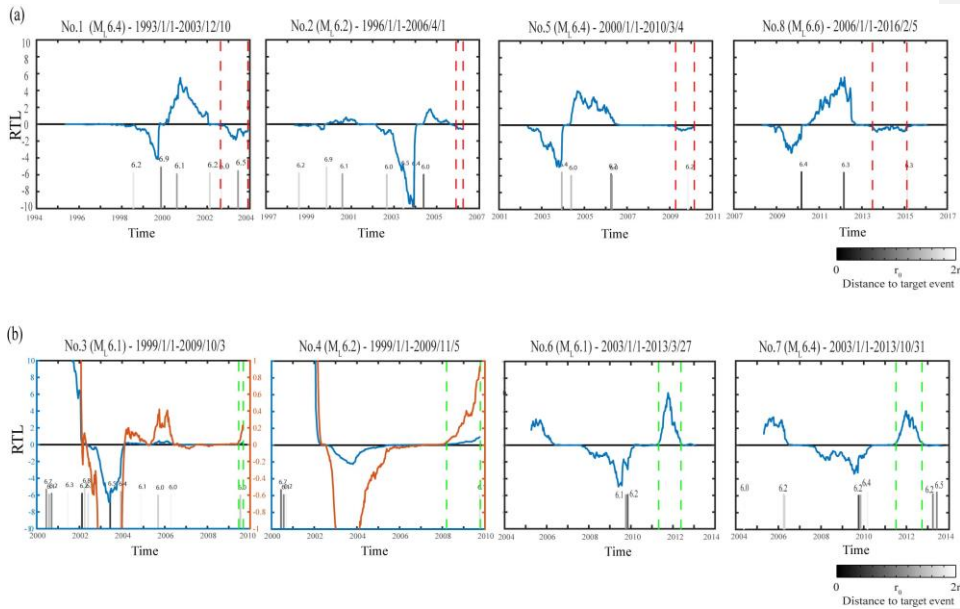


Figure 2: Temporal variation of the RTL function (blue line) for (a) Q-type events and (b) A-type events. The orange curves and vertical axes on the right represent the enlarged RTL functions of event Nos. 3 and 4. The vertical dashed red lines mark the seismic quiescence stage, and the vertical dashed green lines mark the seismic activation stage. The bar chart represents the occurrence time of $M \geq 6.0$ events within a distance of $2r_0$ from the target event; each number above the bar is the magnitude.

137

138 A-type events all occurred in central Taiwan and were located within $2\tilde{r}_0$ with
 139 respect to the 1999 Chi-Chi earthquake. Figure 3 shows the declustered seismicity
 140 distribution as a function of time and latitude. Significant seismicity followed the 1999

141 Chi-Chi earthquake north of 23°N. Since the background seismicity of event Nos. 3 and
 142 4 started from 1999/01/01, the RTL functions were obviously affected by the occurrence
 143 of the 1999 Chi-Chi earthquake. Therefore, we enlarge the vertical axis to accentuate
 144 the seismicity variation prior to event Nos. 3 and 4. As shown in Fig. 2, the temporal
 145 RTL functions of A-type events mostly show a seismic activation stage between 2004
 146 and 2006, which corresponds to the seismicity increase following the 2003 Chengkung
 147 mainshock (event No. 1). However, for the A-type event, we could not see the
 148 relationship between the length of the seismic activation stage and the magnitude.

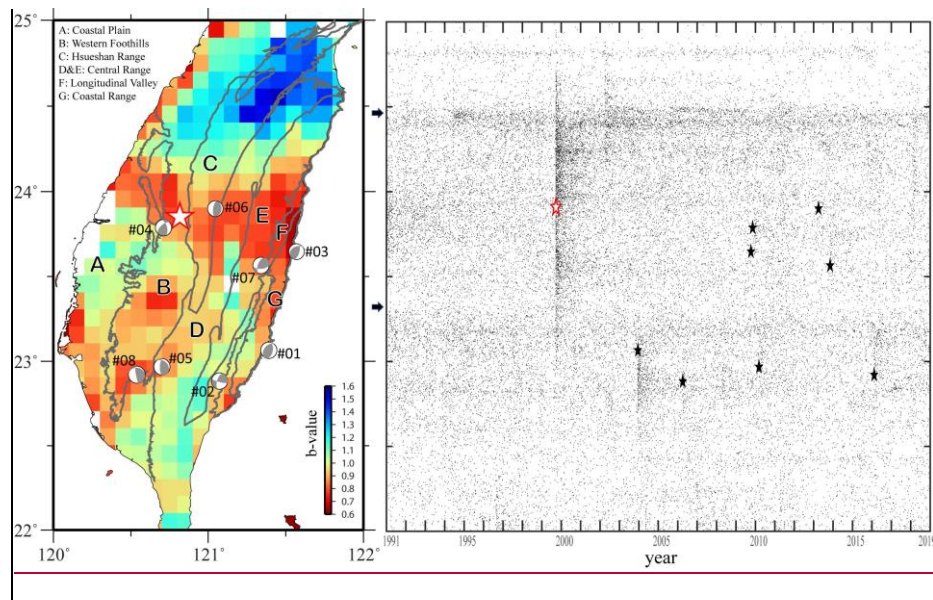


Figure 3: Map view of the earthquake b-value and declustered seismicity distribution as a function of time and latitude. The white star indicates the 1999 Chi-Chi earthquake, and the black stars (or focal mechanisms) represent the investigated events in this study. The black arrows indicate the seismicity boundaries. The major geological units in Taiwan are marked by gray curves and labeled from A to G.

149

150 3.2 Spatial Seismic Activation/Quiescence Distribution

151 Since Q-type and A-type events are located in southern and central Taiwan,
 152 respectively, it would be worth examining the spatial pattern of their abnormal

153 seismicity stages. Wen and Chen (2017) pointed out that various seismic activation or
154 quiescence processes of about 2–4 years were found prior to some events occurring in
155 Taiwan (Chen and Wu, 2006; Wen et al., 2016; Wu et al., 2008). Thus, for consistency,
156 we only consider the last abnormal stage within four years prior to the investigated
157 events, as marked by red vertical lines for the quiescence stage of Q-type events and
158 green vertical lines for the activation stage of A-type events. Then, we calculate the
159 summation of the selected period to generate the seismic quiescence/activation
160 distribution. Considering the definition of the weighted RTL function, a sufficient
161 amount of background seismicity should be regarded as a criterion (Wen and Chen,
162 2017). Using the declustered catalog from 1991 to 2016, we set up two conditions
163 similar to those of Wen and Chen (2017) for each grid to strengthen the reliability: (i)
164 the total number of events within the grid area of $0.1^\circ \times 0.1^\circ$ must be more than 26 (i.e.,
165 at least 1 event occurred every year on average); and (ii) the total events within a circle
166 of $2r_0$ in radius must be more than 9360 (i.e., at least 30 events occurred every month
167 on average). For each event, we normalize the spatial distribution based on the summed
168 result. The spatial seismic activation/quiescence map provides the information of
169 influence of surrounding seismicity state to the target event during the abnormal stage.
170 Similar to previous studies (e.g., Huang et al., 2001; Huang and Ding, 2012), Fig. 4
171 shows that Q-type events mostly occurred on the edge of the seismic quiescence area;
172 and seismic activation appeared around the A-type events.

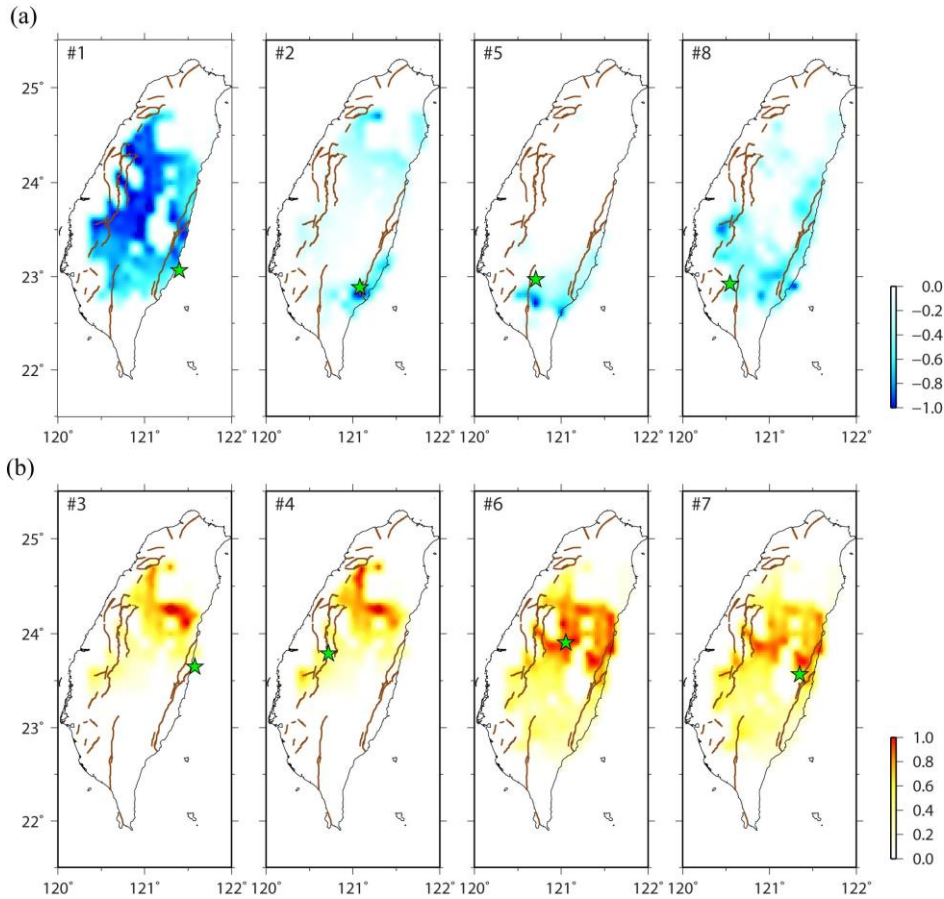


Figure 4: (a) The summed and normalized seismic quiescence map for the selected time window of the temporal RTL function of Q-type events, and (b) the summed and normalized seismic activation map for the selected time window of the temporal RTL function of A-type events. Stars represent the locations of the investigated events. The active faults (thick lines) identified by the Central Geological Survey of Taiwan are also shown.

173

174 4. Discussion

175 4.1 Spatiotemporal Characteristics of Seismicity Changes

176 The RTL analysis accounts for the background seismicity prior to the investigated
 177 event. Therefore, the RTL analyses account for almost the same background period for
 178 event Nos. 3 and 4 (1999-2009) and for event Nos. 6 and 7 (2003-2013), respectively.

179 As the temporal RTL functions show the seismic activation stage prior to the
180 mainshocks during a similar period, we could expect similar seismic activation maps for
181 event Nos. 3 versus 4 and event Nos. 6 versus 7, as shown in Fig. 4. Furthermore, the
182 seismic quiescence stage of event No. 5 occurred in a similar period as the seismic
183 activation stage of event No. 3 (Fig. 2), and the seismic quiescence area of event No. 5
184 complements the seismic activation area of event No. 3 (Fig. 4). In contrast, although
185 event Nos. 3 and 7 occurred at close locations, the difference in the 10-year background
186 period affects the weighting of the deviation. For example, the seismic quiescence stage
187 during 2007–2009 shown in the temporal RTL function of event No. 7 (Fig. 2) is
188 evaluated as the background seismicity level (RTL value is equal to zero) in the temporal
189 RTL function with respect to event No. 3. On the other hand, Wen and Chen (2017)
190 pointed out that an abnormal seismic stage derived with various background periods
191 cannot be produced by chance. The temporal RTL functions of five events (Nos. 1–5 in
192 Fig. 2) accounting for different background periods all exhibit the seismic quiescence
193 stage before the occurrence of event No. 1. This phenomenon is consistent with the
194 seismic quiescence map of event No. 1 (Fig. 4) and the Z-value map of Wu et al. (2008)
195 in which the seismic activity decreased during 2002–2003 for a large area in Taiwan. In
196 addition, the widespread seismic activation distribution of Nos. 6 and 7 (Fig. 4) also
197 responded to the seismic activity increase during 2011–2012 (Nos. 6–8 in Fig. 2). [Wen](#)
198 [et al. \(2016\) suggested that, after the 2010 Jiashian earthquake \(event No. 5\), the 2-year](#)
199 [seismicity increase is caused by the increase in Coulomb stress change, which is](#)
200 [consistent with the seismic activation period in the temporal RTL function of event No.](#)
201 [8.](#)

202 Rundle et al. (2000) proposed the self-organizing spinodal (SOS) model for
203 characteristic earthquakes and suggested that small earthquakes occurred uniformly at

204 all times, while the occurrence rate of intermediate-sized earthquakes varied during the
 205 earthquake cycle. Chen (2003) investigated the SOS behavior of the 1999 Chi-Chi
 206 earthquake and proposed the seismic activation of moderate-size ($5 < M < 6$) events prior
 207 to the mainshock. Here, we also calculate the cumulative frequency–magnitude
 208 distributions for these eight events using the same catalog periods of the RTL analysis.
 209 For each investigated event, we only compared the distribution diagrams of the long-
 210 term (background period) and abnormal seismic stages marked by dashed lines in Fig.
 211 2, within a radius of 25 km with respect to the epicenter. As shown in Fig. 5, cumulative
 212 frequency-magnitude distributions of long-term seismicity (red dots) generally exhibit
 213 linear power law distributions. For the Q-type events, the cumulative frequency
 214 distributions of the seismic quiescence stage (black dots) appear to lack $2.5 < M < 4.5$
 215 events (Fig. 5a), and the lack of a level corresponds to the seismic quiescence
 216 distribution near the epicenter (Fig. 4). This indicates that within the seismic quiescence
 217 stage before the occurrence of the Q-type event, the quiescence of $2.5 < M < 4.5$ activity
 218 contributes to the accumulation of tectonic stress.

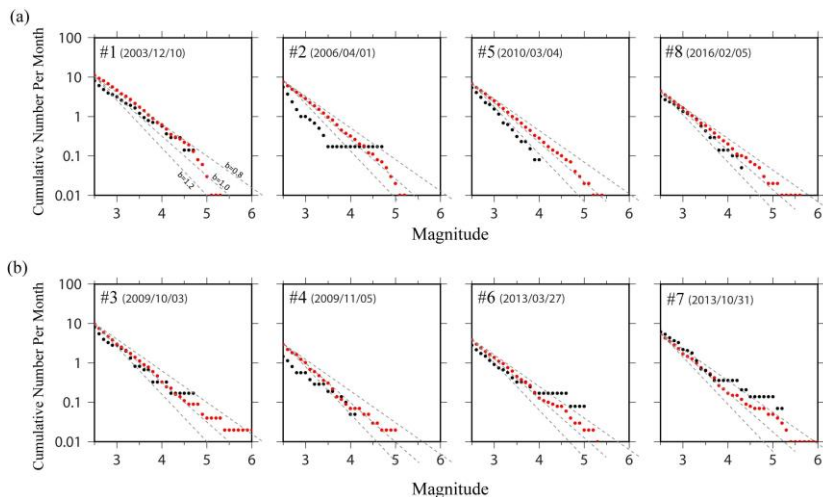


Figure 5: The cumulative frequency–magnitude distributions prior to the investigated events. Red and black dots represent the long-term and abnormal seismic stage marked in Fig. 2, respectively.

219

220 On the other hand, the cumulative frequency distributions of the seismic activation stage
221 of the A-type events (black dots in Fig. 5b) show that the seismic activation of $3 < M < 5$
222 events within the seismic activation stage before the occurrence of the A-type
223 earthquake can be found, which is similar to the results of the 1999 Chi-Chi earthquake
224 (Chen, 2003). Event Nos. 6 and 7, which are located very close to the high seismic
225 activation area (Fig. 4), display the more obvious increase in the number of $4 < M < 5$
226 events during the seismic activation stage (Fig. 5b).

227 Event No. 4 occurred only one month later than event No. 3; however, the seismic
228 activation stage of event No. 4 was much longer than that of event No. 3. Furthermore,
229 the cumulative frequency distributions of the seismic activation stage of event No. 4
230 display a lower intercept (Fig. 5b), which represents the overall decreasing seismicity
231 within this seismic activation stage. Here, we further divide the seismic activation stage
232 of event No. 4 into three periods for discussion: (i) P1: 2008/02–2009/03 before the
233 seismic activation stage of event No. 3; (ii) P2: 2009/04–2009/09 matching the seismic
234 activation stage of event No. 3; and (iii) P3: 2009/10 between the occurrences of event
235 Nos. 3 and 4. The seismic activation distributions in Fig. 6 are all normalized with
236 respect to the maximum RTL value of the seismic activation distribution of event No. 4
237 through Periods P1–P3. We can see that before the seismic activation stage of event No.
238 3 during 2008/02–2009/03 (P1), the location of event No. 3 indeed shows no seismic
239 activation, as exhibited in the temporal RTL function (Fig. 2b). On the other hand, for
240 the location of event No. 4, the seismic activation remains through all three Periods P1–
241 P3. Combined with the overall decreasing seismicity indicated by the lower intercept in
242 Fig. 5(b), these results suggest that this seismic activation prior to event No. 4 was
243 mainly contributed by the relatively accelerating activity of $3.5 < M < 4$ events.

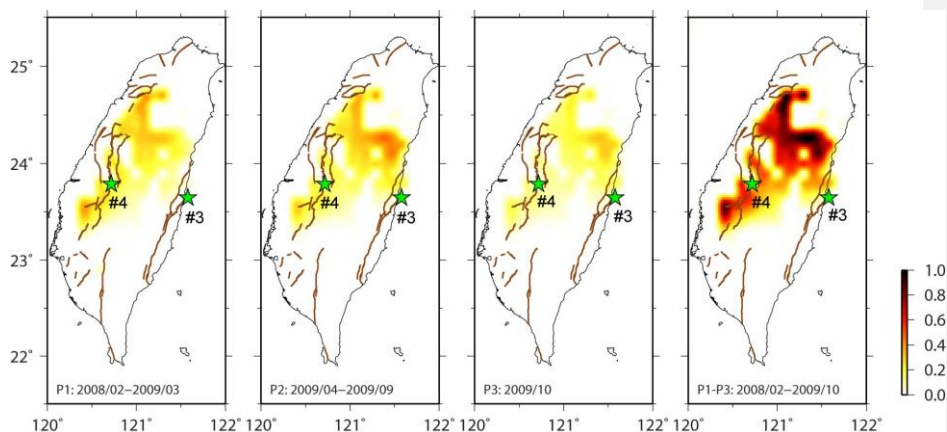


Figure 6: The summed seismic activation map for different periods of the seismic activation stage prior to event No. 4; all maps are normalized based on the summed results of P1–P3. Stars represent the locations of event Nos. 3 and 4. The active faults (thick lines) identified by the Central Geological Survey of Taiwan are also shown.

244

245 **4.2 Implication for the Tectonic Setting**

246 Several major active faults in southwestern Taiwan have been identified, and most
 247 of them have been dominated by thrust movement. Some strike-slip structures, e.g., the
 248 Zuochen and Hsinhua faults, acted as the transfer structures between these thrust faults
 249 (Ching et al., 2011; Deffontaines et al., 1994, 1997; Rau et al., 2012). These transfer
 250 structures develop at around 23°N, which is the northern limit of the Wadati–Benioff
 251 zone (Kao et al., 2000) and close to the seismicity boundary indicated in Fig. 3. Geodetic
 252 data displayed various rates and orientations of horizontal shortening with rapid uplift
 253 rates in southern Taiwan (Fig. 1), which might be caused by underplating beneath the
 254 Central Range sustaining crustal thickening and exhumation (Simoes et al., 2007). The
 255 seismic b-value, which is the relative earthquake size distribution, can be derived from
 256 the Gutenberg–Richter relation (Gutenberg and Richter, 1944): $\log N = a - bM$, where
 257 constant a is related to seismicity and N is the number of earthquakes with magnitudes
 258 greater than M . In general, a high b-value indicates a larger proportion of small events,

259 and a low b-value suggests that large earthquakes dominate over small ones. Using the
260 same declustered catalog from 1991 to 2018, we search for events within a radius of 25
261 km with respect to the center of each grid ($0.1^\circ \times 0.1^\circ$). Only for the grids with more than
262 30 events, we calculate the b-value using the weighted least-squares fitting method (Shi
263 and Bolt, 1982) and the spatial distribution of b-values, as shown in Fig. 3. The
264 seismicity in the southern Central Range is active but shows significant heterogeneity
265 in faulting types (Fig. 1; Chen et al., 2017; Wu et al., 2018), and relatively high b-values
266 suggest the predominance of small earthquakes in this region (Fig. 3 and red dots in Fig.
267 5a; Wu et al., 2018). Wen et al. (2016) found the decreased seismicity and increased
268 Coulomb stress change in the southern Central Range prior to the 2010 Jiashian
269 earthquake (i.e., event No. 5) and suggested both variations in Coulomb stress and
270 seismicity rate play important roles in contributing to the nucleation process of
271 impending earthquakes. The seismicity rate change can be considered a proxy for the
272 stress state change (Dieterich, 1994; Dieterich et al., 2000), and this implies that the
273 quiescence of seismicity contributes to the accumulation of tectonic stress. Since this
274 relatively high b-value region in the southern Central Range has been observed to have
275 a seismicity decrease ($2.5 < M < 4.5$ events) before the occurrence of Q-type events, it can
276 be an indicator of stress change.

277 Many devastating earthquakes with surface ruptures have occurred in the central
278 Taiwan, including the 1935 M 7.1 Hsinchu–Taichung earthquake, the 1951
279 Longitudinal Valley earthquake sequence and the 1999 Chi-Chi earthquake (Lee et al.,
280 2007; Chen et al., 2008; Lin et al., 2013). Hsu et al. (2009) derived the consistent
281 orientations of principal strain-rate and crust stress axes in central Taiwan, which
282 implies that faulting style corresponds to stress buildup accumulating from interseismic
283 loading (Fig. 1). They also pointed out that, for central Taiwan, small events tend to

284 surround the locked fault zone, where major earthquakes might occur, during the
285 interseismic period. The 1999 Chi-Chi earthquake ruptured the area near the end of the
286 décollement with a high contraction rate (Dominguez et al., 2003; Hsu et al., 2003;
287 2009). In addition, similar to the 1999 Chi-Chi earthquake, the A-type events occurred
288 in the low b-value area surrounded by small and active events. Chen and Wu (2006)
289 derived the temporal RTL function of the 1999 Chi-Chi earthquake, showing a pattern
290 similar to that of A-type events with the activation stage prior to the mainshock.
291 Furthermore, Wu (2006) calculated the seismic activation map of the 1999 Chi-Chi
292 event and found that the 1999 Chi-Chi mainshock occurred on the edge of the seismic
293 activation area, which is a low b-value region. This is similar to the seismic activation
294 maps of A-type events, which display the hot-spot pattern contracting within the low b-
295 value area (Figs. 3 and 4). The nucleation of the A-type mainshock can be attributed to
296 the perturbation of background seismicity ($3 < M < 5$ events) by the stress state change
297 (Dieterich, 1994; Dieterich et al., 2000).

298 The cumulative frequency distributions of long-term seismicity in Fig. 5 show a b-
299 value of 0.8–1.0 around these eight events, which is consistent with the pattern shown
300 in Fig. 3. However, the cumulative frequency distributions of long-term seismicity
301 exhibit different trends of magnitudes larger than 4.5 for the two types of events. The
302 seismicity for $M > 4.5$ events is lower in the area around the Q-type event but higher in
303 the area around the A-type event. Event Nos. 1, 2, 3 and 7 occurred in eastern Taiwan
304 with an average GPS velocity of about 60 mm/yr (Fig. 1), and the cumulative frequency
305 distributions of long-term seismicity display a high intercept (Fig. 5). This rapid
306 convergence rate generally remains in the western part of southern Taiwan, which
307 indicates that only a little shortening is consumed from east to the west in southern
308 Taiwan. This corresponds to the active seismicity of small earthquakes, as indicated by

309 the high intercept of the cumulative frequency distributions of long-term seismicity for
310 event Nos. 1, 2, 5 and 8 (Fig. 5). Therefore, for the pre-collisional rapid and
311 distributed convergence in southern Taiwan (Shyu et al., 2005a), the quiescence of
312 $2.5 < M < 4.5$ activity contributes to the accumulation of tectonic stress for preparing for
313 the occurrence of the Q-type event. On the other hand, the shortening rate is obviously
314 consumed in the mountainous area of central Taiwan. Therefore, the lowest intercept of
315 the cumulative frequency distributions of long-term seismicity for event No. 4 (Fig. 5)
316 reflects the slow GPS velocity and low seismicity in the western part of central Taiwan
317 (Fig. 1). For central Taiwan, small events tend to surround the locked fault zone of the
318 potential major events during the interseismic period, and the 1999 Chi-Chi earthquake
319 is the case affected by the accelerating seismicity of moderate-size events and ruptured
320 the area near the end of the décollement with a high contraction rate (Chen, 2003;
321 Dominguez et al., 2003; Hsu et al., 2003; 2009). Tectonic stress accumulating from the
322 interseismic loading with the perturbation of the accelerating activity of $3 < M < 5$ events
323 could promote the nucleation process of the A-type event. The mechanisms causing
324 these different phenomena are not clear, and further study is still needed. For example,
325 some studies using machine-learning-based earthquake detectors and template-
326 matching techniques will be helpful to build a more complete earthquake catalog in
327 Taiwan (Liao et al., 2021; Zhai et al., 2021) and to get more useful data on small
328 earthquakes with a magnitude below 2.5.

329

330 5. Conclusion

331 Through statistical analyses of recent large earthquakes that occurred in Taiwan, we
332 summarize various temporal and spatial seismicity patterns prior to the earthquakes that
333 nucleated in different regions of Taiwan:

- 334 • Q-type events occurred in southern Taiwan, with the northern boundary of
335 23.2°N, and experienced a seismic quiescence stage prior to the mainshock.
336 A seismicity decrease of $2.5 < M < 4.5$ events in the relatively high b-value
337 southern Central Range could be an indicator of stress change related to the
338 preparation process of such events.
- 339 • A-type events occurred in central Taiwan and experienced a seismic
340 activation stage prior to the mainshock, which nucleated on the edge of the
341 seismic activation area. We should consider when accelerating seismicity
342 of $3 < M < 5$ events appears within the low b-value area.

343 Our results show that the spatiotemporal seismicity variations during the
344 preparation process of impending earthquakes could display a distinctive pattern
345 corresponding to the tectonic setting. ~~However, the mechanisms causing these different~~
346 ~~phenomena are not clear, and further study is still needed.~~

347
348

349 Appendix A

350 In the systematic correlation analysis for searching the optimal model parameters,
 351 we calculate various combinations of r_0 (ranging between 25 and 80 km with a step of
 352 2.5 km) and t_0 (ranging between 0.25 and 2.0 yr with a step of 0.05 yr). As the correlation
 353 coefficient criterion C_0 is set, we can calculate the ratio W (or weight) of the combination
 354 with correlation coefficients equal to or larger than C_0 for each model parameter of r_{0i}
 355 ($i=1\sim m; m=23$) and t_{0j} ($j=1\sim n; n=36$). Then, the contour map for the ratio W is generated,
 356 as shown in Fig. A1.

$$357 \quad W_{ij} = \frac{\sum_{k=1}^m I(C_{ik} \geq C_0) + \sum_{l=1}^n I(C_{jl} \geq C_0)}{m+n} \quad (A1)$$

358 where the logical function $I(\Phi)$ is defined as

$$359 \quad I(\Phi) = \begin{cases} 1, & \Phi \text{ is true} \\ 0, & \text{otherwise} \end{cases} \quad (A2)$$

360 As the criterion ratio W_0 is set, the optimal model parameters, \tilde{r}_0 and \tilde{t}_0 , can be
 361 obtained by the following formulas:

$$362 \quad \tilde{r}_0 = \frac{\sum_{j=1}^n \sum_{i=1}^m W_{ij} I(W_{ij} \geq W_0) r_{0i}}{\sum_{j=1}^n \sum_{i=1}^m W_{ij} I(W_{ij} \geq W_0)} \quad (A3)$$

$$363 \quad \tilde{t}_0 = \frac{\sum_{i=1}^m \sum_{j=1}^n W_{ij} I(W_{ij} \geq W_0) t_{0j}}{\sum_{i=1}^m \sum_{j=1}^n W_{ij} I(W_{ij} \geq W_0)} \quad (A4)$$

364 Using event No. 6 as an example, we considered criterion coefficient $C_0 = 0.6$ and
 365 criterion ratio $W_0 = 0.5$, which indicates that at least 50% of the total combination pairs
 366 had a correlation coefficient $C \geq C_0 = 0.6$. Then, we obtained $\tilde{r}_0 = 50.0$ km and $\tilde{t}_0 = 1.14$
 367 yr (diamond in Fig. A1) by averaging the parameter values that passed the criterion.

368 In addition, Nagao et al. (2011) proposed the RTM algorithm to reduce the dual
 369 effect of the distance (r_i) by introducing the new factor

$$370 \quad M(x, y, z, t) = [\sum_{i=1}^n (M_i)] - M_{bk}(x, y, z, t) \quad (A4)$$

371 where M_i is the earthquake magnitude of the i th prior event. Here, we also calculate the
 372 RTM function of each investigated event with the same characteristic parameter set of
 373 the RTL model, and both functions display very similar trends with minor differences,
 374 as shown in Figure R2. The reason for this could be that, for these eight events, no large
 375 earthquakes occurred in the vicinity of the epicenter. The bar chart in Fig. A2, which

376 represents the occurrence time of $M \geq 6.0$ events within a distance of $2r_0$ from the target
 377 event, also supports this explanation.

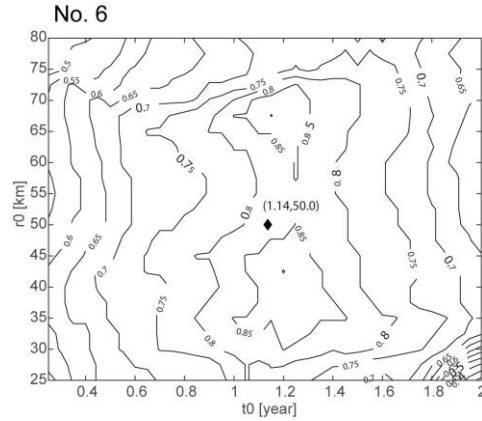


Figure A1: Contour map of ratio W for various combinations of model parameters of r_0 and t_0 , with $C_0 = 0.6$ for event No. 6. The diamond shows the optimal model parameters as selecting criterion ratio $W_0 = 0.5$.

378
 379

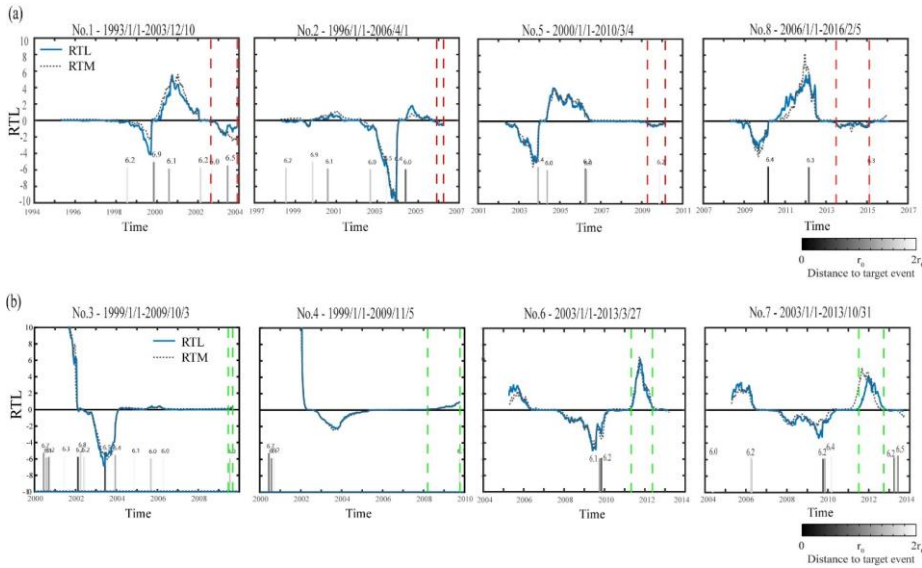


Figure A2: Temporal variation of the RTL (solid line) and RTM (dotted line) functions for (a) **QA**-type events and (b) **BA**-type events. The bar chart represents the occurrence time of $M \geq 6.0$ events within a distance of $2r_0$ from the target event; each number above the bar is the magnitude.

380 **Data Availability** : The seismic data is available in the Geophysical Database
381 Management System (GDMS, <https://gdms.cwb.gov.tw/>). A Chinese manual for data
382 access from the GDMS is on the website.

383

384 **Author contributions**: Conceptualisation, YYW, CCC; Investigation, YYW, WTL;
385 Validation, Formal analysis, Writing - original draft preparation, YYW; Writing -
386 review & editing, YYW, CCC, SW.

387

388 **Competing interests**: The authors declare no conflicts of interest.

389

390 **Acknowledgments**: We thank Central Weather Bureau (CWB) of Taiwan for providing
391 seismic data. This research was supported by the Ministry of Science and Technology
392 in Taiwan with grant: MOST 110-2116-M-194-018. The Taiwan Earthquake Center
393 (TEC) contribution number for this article is ****.

394

395

396 **References:**

- 397 Chan, C.H., Wu, Y.M., Tseng, T.L., Lin, T.L., and Chen, C.C.: Spatial and temporal
398 evolution of b-values before large earthquakes in Taiwan. *Tectonophysics*, **532**,
399 215-222, 2012.
- 400 Chen, C.-C., Rundle, J.B., Holliday, J.R., Nanjo, K.Z., Turcotte, D.L., Li, S.C., and
401 Tiampo, K. F.: The 1999 Chi-Chi, Taiwan, earthquake as a typical example of
402 seismic activation and quiescence. *Geophys. Res. Lett.*, **32**(22), L22315,
403 doi:10.1029/2005GL023991, 2005.
- 404 Chen, C.C., and Wu, Y.X.: An improved region–time–length algorithm applied to the
405 1999 Chi-Chi, Taiwan earthquake. *Geophys. J. Int.*, **166**, 1144-1147, doi
406 10.1111/j.1365-246X.2006.02975.x, 2006.
- 407 Chen, J.S., Ching, K.E., Rau, R.J., Hu, J.C., Cheng, K.C., Chang, W.L., Chuang, R.Y.,
408 Chen, C.L., and Chen, H.C.: Surface deformation in Taiwan during 2002-2017
409 determined from GNSS and precise leveling measurements. Central Geological
410 Survey Special Publication, 33, 157-178, 2018. (in Chinese with English abstract)
- 411 Chen, K.H., Toda, S., and Rau, R.J.: A leaping, triggered sequence along a segmented
412 fault: the 1951 Hualien – Taitung earthquake sequence in eastern Taiwan. *J.*
413 *Geophys. Res.*, **113**, B02304, doi:10.1029/2007JB005048, 2008.
- 414 Chen, S.K., Wu, Y.M., Hsu, Y.J., and Chan, Y.C.: Current crustal deformation
415 reassessed by cGPS strain-rate estimation and focal mechanism stress inversion.
416 *Geophys. J. Int.*, **210**, 228–239. <https://doi.org/10.1093/gji/ggx165>, 2017.
- 417 Ching, K.E., Johnson, K.M., Rau, R.J., Chuang, R.Y., Kuo, L.C., and Leu, P.L.: Inferred
418 fault geometry and slip distribution of the 2010 Jiashian, Taiwan, earthquake is
419 consistent with a thick-skinned deformation model. *Earth Planet. Sci. Lett.*, EPSL-
420 S-10-00445, doi:10.1016/j.epsl.2010.10.021, 2011.

421 Deffontaines, B., Lee, J.-C., Angelier, J., Carvalho, J., and Rudant, J.-P.: New
422 geomorphic data on the active Taiwan orogen: a multisource approach. *J. Geophys.*
423 *Res.*, **99**, 20243–20266, 1994.

424 Deffontaines, B., Lacombe, O., Angelier, J., Mouthereau, F., Lee, C.T., Deramond, J.,
425 Lee, J.F., Yu, M.S., and Liu, P.M.: Quaternary transfer faulting in Taiwan Foothills:
426 evidence from a multisource approach. *Tectonophysics*, **274**, 61–82, 1997.

427 Dieterich, J. H.: A constitutive law for rate of earthquake production and its application
428 to earthquake clustering. *J. Geophys. Res.*, **99** (18), 2601-2618, 1994.

429 Dieterich, J., Cayol, V., and Okubo, P.: The use of earthquake rate changes as a stress
430 meter at Kilauea volcano. *Nature*, **408**, 457–460, 2000.

431 Dominguez, S., Avouac, J.P., and Michel, R.: Horizontal coseismic deformation of the
432 1999 Chi-Chi earthquake measured from SPOT satellite images: implications for
433 the seismic cycle along the western foothills of central Taiwan. *J. Geophys. Res.*,
434 **108**, doi:10.1029/2001JB000951, 2003.

435 Gardner, J. K., and Knopoff, L.: Is the sequence of earthquakes in Southern California,
436 with aftershocks removed, Poissonian?. *Bull. Seis. Soc. Am.*, **64**(5), 1363-1367,
437 1974.

438 Gutenberg, B., and Richter, C.F.: Frequency of earthquakes in California. *Bull. seism.*
439 *Soc. Am.*, **34**, 185–188, 1944.

440 Hsu, Y.J., Kao, H., Bürgmann, R., Lee, Y.T., Huang, H.H., Hsu, Y.F., and Zhuang, J.:
441 Synchronized and asynchronous modulation of seismicity by hydrological loading:
442 A case study in Taiwan. *Sci. Adv.*, **7** (16), p. eabf7282, doi: 10.1126/sciadv.abf7282,
443 2021.

444 Hsu, Y.J., Simons, M., Yu, S.B., Kuo, L.C., and Chen, H.Y.: A two-dimensional
445 dislocation model for interseismic deformation of the Taiwan mountain belt. *Earth*
446 *Planet. Sci. Lett.*, **211**, 287–294, 2003.

447 Hsu, Y.J., Yu, S.B., Simons, M., Kuo, L.C., and Chen, H.Y.: Interseismic crustal
448 deformation in the Taiwan plate boundary zone revealed by GPS observations,
449 seismicity, and earthquake focal mechanisms. *Tectonophysics*, **479**, 4–18.
450 <https://doi.org/10.1016/j.tecto.2008.11.016>, 2009.

451 Huang, Q., and Ding, X.: Spatiotemporal variations of seismic quiescence prior to the
452 2011 M 9.0 Tohoku earthquake revealed by an improved Region-Time-Length
453 algorithm. *Bull. Seismol. Soc. Am.*, **102**(4), 1878-1883, doi: 10.1785/0120110343,
454 2012.

455 Huang, Q., Sobolev, G.A., and Nagao, T.: Characteristics of the seismic quiescence and
456 activation patterns before the M=7.2 Kobe earthquake. *Tectonophysics*, **337**, 99-
457 116, 2001.

458 Kao, H., Huang, G.C., and Liu, C.S.: Transition from oblique subduction to collision in
459 the northern Luzon arc-Taiwan region: Constraints from bathymetry and seismic
460 observations. *J. Geophys. Res.*, **105**, 3059-3079, 2000.

461 Kasahara, K.: Earthquake Mechanics, *Cambridge Univ. Press., Cambridge*, 248 pp.,
462 1981.

463 Lee, S.J., Chen, H.W., and Ma, K.F.: Strong Ground Motion Simulation of the 1999
464 Chi-Chi, Taiwan, Earthquake from a Realistic 3D Source and Crustal Structure. *J.*
465 *Geophys. Res.*, **112**, B06307, doi: 10.1029/2006JB004615, 2007.

466 Liao, W. Y., Lee, E. J., Mu, D., Chen, P., and Rau, R. J.: ARRU phase picker: Attention
467 recurrent-residual U-Net for picking seismic P-and S-phase arrivals. *Seismol. Res.*
468 *Lett.*, **92**(4), 2410-2428, 2021.

Formatted: Font: Italic

Formatted: Font: Bold

469 Lin, D.-H., Chen, H., Rau, R.-J., and Hu, J.-C.: The role of a hidden fault in stress
470 triggering: Stress interactions within the 1935 Mw 7.1 Hsinchu–Taichung
471 earthquake sequence in central Taiwan. *Tectonophysics*, **601**, 37-52, doi:
472 10.1016/j.tecto.2013.04.022, 2013.

473 Lu, W. T.: Seismicity Changes Prior to the M>6 Earthquakes in Taiwan During 1993 to
474 2016 - an Approach of the RTL Algorithm. M.Sc. thesis, National Chung Cheng
475 University, Taiwan, p 66, 2017. (in Chinese with English abstract)

476 Mignan, A., and Giovambattista, R. Di: Relationship between accelerating seismicity
477 and quiescence, two precursors to large earthquakes. *Geophys. Res. Lett.*, **35**,
478 L15306, doi:10.1029/2008GL035024, 2008.

479 Rau, R.J., Lee, J.C., Ching, K.E., Lee, Y.H., Byrne, T.B., and Chen, R.Y.: Subduction-
480 continent collision in southwestern Taiwan and the 2010 Jiashian earthquake
481 sequence. *Tectonophysics*, **578**, 107-116, doi:10.1016/j.tecto.2011.09.013, 2012.

482 Rundle, J.B., Klein, W., Turcotte, D.L., and Malamud, B.D.: Precursory seismic
483 activation and critical point phenomena. *Pure Appl. Geophys.*, **157**, 2165-2182,
484 doi:10.1007/PL00001079, 2000.

485 Simoes, M., Avouac, J.P., Beyssac, O., Goffe, B., Farley, K.A., and Chen, Y.G.:
486 Mountain building in Taiwan: a thermokinematic model. *J. Geophys. Res.*, **112**.
487 doi:10.1029/2006JB004824, 2007.

488 Shi, Y., and Bolt, B.A.: The standard error of the magnitude-frequency b value. *Bull.*
489 *seism. Soc. Am.*, **72**, 1677–1687, 1982.

490 Shyu, J. B. H., Sieh, K., and Chen, Y.-G.: Tandem suturing and disarticulation of the
491 Taiwan orogen revealed by its neotectonic elements. *Earth Planet. Sci. Lett.*, **233**,
492 167–177, 2005a.

493 Shyu, J.B.H., Sieh, K., Chen, Y.-G., and Liu, C.-S.: Neotectonic architecture of Taiwan
494 and its implications for future large earthquakes. *J. Geophys. Res.*, **110**, p. B08402,
495 doi: 10.1029/2004JB003251, 2005b.

496 Sobolev, G.A., and Tyupkin, Y.S.: Low-seismicity precursors of large earthquakes in
497 Kamchatka. *Volc. Seismol.*, **18**, 433-446, 1997.

498 Sobolev, G.A., and Tyupkin, Y.S.: Precursory phases, seismicity precursors, and
499 earthquake prediction in Kamchatka. *Volc. Seismol.*, **20**, 615-627, 1999.

500 Suppe, J.: Kinematics of arc-continent collision, flipping of subduction, and backarc
501 spreading near Taiwan. *Mem. Geol. Soc. China*, 21–33, 1984.

502 Wang, J.H.: The Taiwan Telemetered Seismographic Network. *Phys. Earth Planet.*
503 *Inter.*, **58**, 9–18, 1989

504 Wang, J.H., Chen, K.C., and Lee, T.Q.: Depth distribution of shallow earthquakes in
505 Taiwan. *J. Geol. Soc. China*, **37**, 125–142, 1994.

506 Wen, Y.-Y., Chen, C.-C., Wu, Y.-H., Chan, C.-H., Wang, Y.-J., and Yeh, Y.-L.:
507 Spatiotemporal investigation of seismicity and Coulomb stress variations prior to
508 the 2010 ML 6.4 Jiashian, Taiwan earthquake. *Geophys. Res. Lett.*, **43**,
509 doi:10.1002/2016GL070633, 2016.

510 Wen, Y.-Y., and Chen, C.-C.: Seismicity variations prior to the 2016 ML 6.6 Meinong,
511 Taiwan earthquake. *Terr. Atmos. Ocean. Sci.*, **28**, 737-742, doi:
512 10.3319/TAO.2016.12.05.01, 2017.

513 Wu, Y. H.: An improved region–time–length algorithm applied to the 1999 Chi-Chi,
514 Taiwan earthquake. M.Sc. thesis, National Central University, Taiwan, p 115, 2006.
515 (in Chinese with English abstract)

516 Wu, Y.M., and Chiao, L.Y.: Seismic Quiescence before the 1999 Chi-Chi, Taiwan, Mw
517 7.6 Earthquake. *Bull. Seismol. Soc. Am.*, **96**, 321-327, doi: 10.1785/0120050069,
518 2006.

519 Wu, Y.M., Chen, C.-C., Zhao, L., and Chang, C.-H.: Seismicity characteristics before
520 the 2003 Chengkung, Taiwan, earthquake. *Tectonophysics*, **457**, 177-182, doi:
521 10.1016/j.tecto.2008.06.007.

522 Wu, Y.M., Chen, S. K., Huang, T.C., Huang, H.-H., Chao, W.A., and Koulakov, I.:
523 Relationship between earthquake b-values and crustal stresses in a young orogenic
524 belt. *Geophys. Res. Lett.*, **45**, 1832-1837, doi:10.1002/2017GL076694, 2018.

525 Wu, Y.M., Hsu, Y.J., Chang, C.H., Teng, L.S., and Nakamura, M.: Temporal and spatial
526 variation of stress field in Taiwan from 1991 to 2007: Insights from comprehensive
527 first motion focal mechanism catalog. *Earth Planet. Sci. Lett.*, **298**, 306–316.
528 <https://doi.org/10.1016/j.epsl.2010.07.047>, 2010.

529 Wyss, M., and Stefansson, R.: Nucleation points of recent mainshocks in Southern
530 Iceland, mapped by b-values. *Bull. Seismol. Soc. Am.*, **96**, 599–608, 2006.

531 Yu, S.B., Chen, H.Y., and Kuo, L.C.: Velocity field of GPS stations in the Taiwan area.
532 *Tectonophysics*, **274**(1-3), 41–59. [https://doi.org/10.1016/S0040-1951\(96\)00297-1](https://doi.org/10.1016/S0040-1951(96)00297-1),
533 1997.

534 Zhai, Q. S., Peng, Z. G., Chuang, L. Y., Wu, Y. M., Hsu, Y. J., and Wdowinski, S.:
535 Investigating the Impacts of a Wet Typhoon on Microseismicity: A Case Study of
536 the 2009 Typhoon Morakot in Taiwan Based on a Template Matching Catalog. *J.*
537 *Geophys. Res.*, **126**(12). <https://doi.org/10.1029/2021JB023026>, 2021.
538

Formatted: Font: Italic

Formatted: Font: Bold